Chemical Engineering Journal Advances 14 (2023) 100473

Contents lists available at ScienceDirect

Chemical Engineering Journal Advances

journal homepage: www.sciencedirect.com/journal/chemical-engineering-journal-advances

A continuous photo-Fenton-like process using persulfate salts for the degradation of acetaminophen under solar irradiation at circumneutral pH

Bruno Ramos [a,b,*], Lívia Babetto Ferreira [a], Priscila Hasse Palharim [a], Patrícia Metolina [a], Carolina de Araújo Gusmão [a], Antonio Carlos Silva Costa Teixeira [a]

[a] Department of Chemical Engineering, Escola Politécnica, University of São Paulo, 05088000, São Paulo, Brazil
[b] Bionanomanufacturing Center, Instituto de Pesquisas Tecnológicas do Estado de São Paulo, 05508901, São Paulo, Brazil

ARTICLE INFO

Keywords:
Photo-Fenton
Advanced oxidation processes
Persulfate
Solar-driven

ABSTRACT

The demand for sustainable and feasible water treatment technologies (WTT) increases with the growing realization of the magnitude of the damage that our indiscriminate wastewater disposal strategy has caused the Environment. Considering the increasing costs of energy, the development of solar-driven processes is key to ensuring the economic feasibility of WTT for industries of all sizes. In this direction, this paper reports the development of a photo-Fenton-like system based on the persulfate ion and the use of solar irradiation as its coactivator for use in continuous processes. Using acetaminophen as model contaminant (C_0 = 5 ppm), we showed that under optimal conditions and circumneutral pH (pH ~5.6), a removal of 94% was achievable with a residence time of 3.3 min. Economically, this translates into a collector area per order of 11.4 $m^2/(m^3$ order), in line with the best numbers found in the literature. We showed that this was achieved due to the improved concentration of sulfate radicals, $SO_4^{\bullet -}$, formed in the system, when compared to the same process carried out in a small-scale batch reactor. Our results, obtained under controlled conditions using a solar simulator, were validated under natural sunlight, confirming the feasibility of our proposed intensification strategy.

1. Introduction

The presence of pollutants of emerging concern in different water bodies is a global problem that has attracted great interest. It is well known that conventional wastewater treatment processes are not efficient in removing these contaminants, leading to their persistence and accumulation in the environment. Several studies have already proposed different strategies to overcome this issue. Although most of them provide promising results, they are usually limited to the lab scale, mainly due to high implementation costs, the release of possible toxic compounds, or scaling-out difficulties. Thus, there is an urgent need to develop technologies capable of removing contaminants of emerging concern using sustainable ways.

Sustainable effluent treatment technologies involve the use of less intensive processes with a reduced consumption of energy and chemicals. In this context, *advanced oxidation processes* (AOPs) provide interesting alternatives that offer high removal rates with the possibility of using sunlight as a driving force. Most AOPs are based on in situ production of hydroxyl radicals ($HO^{\bullet}$) to remove organic compounds. However, AOPs based on sulfate radicals ($SO_4^{\bullet -}$) have recently gained attention due to their advantages over the $HO^{\bullet}$-based processes, such as the higher oxidation potential ($E^0_{(SO4^{\bullet -})} = 2.5–3.1$ V, compared to $E^0_{(HO^{\bullet})} = 1.7–2.8$ V) and longer lifetime ($t_{1/2\ (SO4^{\bullet -})} = 30–40$ μs, compared to $t_{1/2\ (HO^{\bullet})} = 20$ ns) of the sulfate radicals in aqueous medium [1,2].

Peroxidisulfate, also known as persulfate (PS), is the main precursor used to produce $SO_4^{\bullet -}$ in aqueous solutions. It can be directly activated by UV irradiation, ultrasound, and heat; or indirectly by catalytic activation in the presence of transition metals (Fe, Co, Cu, Ag, Ni, and Mn) or carbon, according to the equations I-II [1–3].

$$S_2O_8^{2-} \xrightarrow{\text{UV/Heat/US}} 2SO_4^{\bullet -} \quad \text{(I)}$$

$$S_2O_8^{2-} + M^{2+} \rightarrow M^{3+} + SO_4^{\bullet -} + SO_4^{2-} \quad \text{(II)}$$

The most widely used activator is iron, metallic or ionic, for a combination of economic (low cost and highly abundant), environmental (negligible toxicity), and technological (highly effective and easily removable from water) reasons [1]. Nevertheless, relatively high concentrations of iron may be required to efficiently activate PS and

* Corresponding author.
E-mail address: bruno.ramos@usp.br (B. Ramos).

https://doi.org/10.1016/j.ceja.2023.100473

Available online 24 February 2023

promote the complete removal of organic pollutants, sometimes exceeding the safe disposal limits [2]. To overcome this problem, processes that combine iron at trace levels with other activators, such as irradiation, are proposed. Such combinations often result in high pollutant removal efficiency and low operational costs [4]. In these chemical systems, the improvement in removal efficiency is generally attributed to direct and indirect (Fe-mediated) photolysis of PS [3,5].

Some systems combining sulfate-based processes with transition metals and irradiation have already been reported and confirm their efficacy. Bandala et al. [6] studied the removal of atrazine by cobalt/-peroximonosulfate activated by natural sunlight in a 60 mL batch reactor. They achieved 66% removal of atrazine in the absence of light (126 min) and 100% removal (75 min) in the presence of sunlight. Ahmed and Chiron [5] evaluated carbamazepine removal by PS/Fe^{2+}/UV–vis using simulated solar irradiation in a stirred cylindrical closed cell and could reach complete removal in 30 min, while < 30% were removed in the absence of light. Khan et al. [4] investigated the removal of atrazine by the UV/H_2O_2/Fe^{2+}, UV/$S_2O_8^{2-}$/Fe^{2+} and UV/HSO_5^-/Fe^{2+} processes, in a batch reactor. The UV/$S_2O_8^{2-}$/Fe^{2+} system was found to be the most efficient at pH 5.8. Nie et al. [7] analyzed the removal of chloramphenicol using UV–vis/PS/Fe^{2+} with simulated solar light, carrying out the experiments in a quartz photochemical batch reactor. The authors achieved only 27.2% removal by the PS/Fe^{2+} system, compared to 96.9% by the UV–vis/PS/Fe^{2+} system, after 100 min of reaction.

As can be seen, these combined systems have achieved high organic compound removal efficiencies, but it should be noted that there is a lack of studies evaluating the use of solar energy and the efficient use of the solar spectrum. Furthermore, the application of a continuous flow process, which would allow a better integration into wastewater treatment plants, has not been reported. Considering this important gap, this work reports on the development of a continuous Sunlight/PS/Fe^{2+} process to remove acetaminophen (ACT), selected as a model contaminant of an important class of aminophenolic pharmaceutical compounds. The influence of PS and Fe^{2+} concentrations on the ACT removal efficiency was evaluated by the two-variable Doehlert experimental design [8]. Finally, for the best reaction conditions, the effect of oxidative species ($HO^{\bullet}$, $SO_4^{\bullet-}$) and the use of solar energy was investigated. To the best of our knowledge, this is the first study to combine all of these features.

2. Investigation approach

2.1. Chemicals

Acetaminophen (ACT), $C_8H_9NO_2$ (≥ 99%, HPLC grade), sodium persulfate (SPS), $Na_2S_2O_8$ (≥ 98%, reagent grade), ferrous sulfate heptahydrate, $FeSO_4{\cdot}7H_2O$ (≥ 99%, ACS reagent), methanol (≥ 99%, HPLC grade), tert-butyl alcohol (≥ 99%, ACS reagent), isopropanol (≥ 99%, HPLC grade) and hydroquinone (≥ 98%, reagent grade) were acquired from Sigma Aldrich and used as received. Acrylonitrile-butadiene-styrene (ABS) filament (⌀ 1.75 mm), prepared from wasted ABS parts, was donated by PrintGreen 3D. Soda-lime glass slides (76 × 26 × 1.2 mm) were thoroughly washed with ethanol and dried prior to use. All solutions were prepared in deionized water.

2.2. Experimental apparatus

A bench-scale continuous photoreaction system was assembled as illustrated in Fig. 1. It consists of one syringe pump (Elite 11, Harvard Apparatus, Inc.) and one metering pump (LC-10AT, Shimadzu Co.), one static micromixer (Shimadzu Co.), one microreactor, and a high-power metal halide lamp (400 W HPI-T, Phillips Co.). The irradiance spectrum provided by the light source at the reactor surface was measured with a spectroradiometer (SPR-4002, Luzchem Research, Inc.) and is reported in the inset of Fig. 1. The reactor was placed 15 cm away from the lamp and inclined 20° with respect to the lamp axis to facilitate the gravitational removal of evolved gas bubbles. This distance was chosen so that the total UV irradiance at the reactor surface equals the ASTM standard AM1.5 G solar irradiation at sea level, ca. 4.6 mW cm^{-2} [9]. The connections between the pumps, the mixer, and the reactor were made using microfluidic Tygon tubings and PTFE connectors.

The 3.0-mL, 10.6 × 4.1 cm microreactor was designed as described elsewhere [10], based on the principles of improved flow distribution, promotion of static mixing, and intensification of light absorption. The equipment was prototyped in ABS by fused filament fabrication using a commercial 3D printer (Creator Pro, Flashforge Inc.) by controlled extrusion at 230 °C on a heated bed (110 °C). Watertightness was

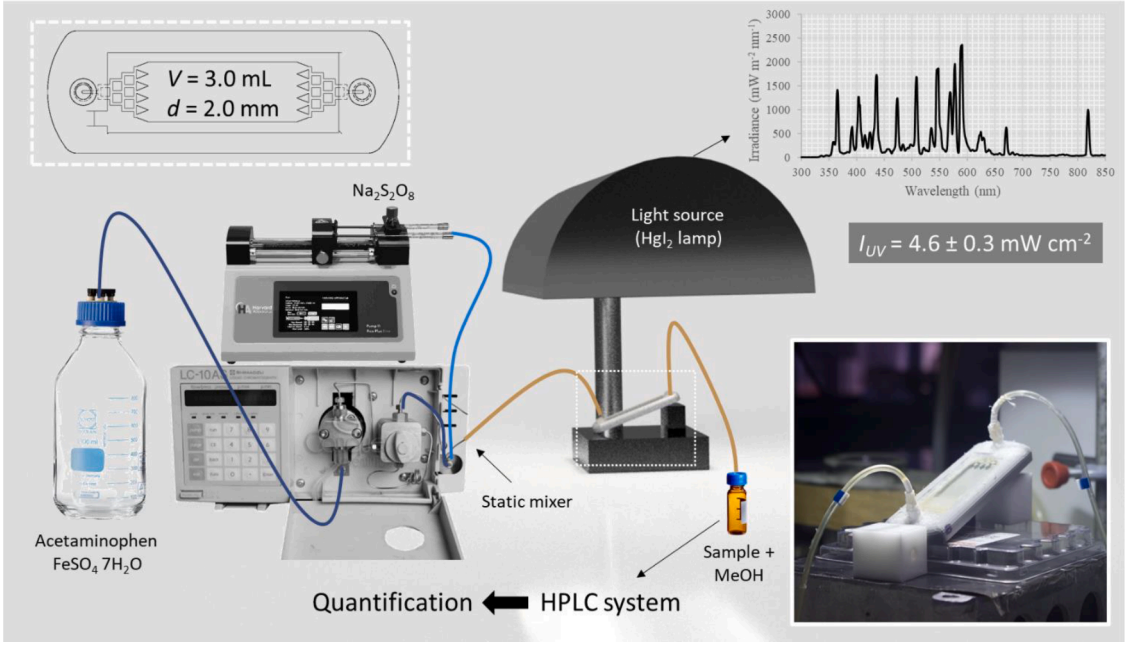

Fig. 1. Experimental apparatus for continuous Fe-assisted solar/PS experiments. The inset pictures show the reactor geometry, the light source emission spectrum, and a photograph of the reactor in operation under simulated sunlight.

ensured using an infill setting of 90% and five solid layers on the flooring of the reaction chamber. An irradiation window (A_{irrad} = 10 cm^2) was provided by a 1.2-mm soda-lime glass slide, appropriately secured with the aid of a suitable amount of acetoxy silicone sealant (Tekbond, Saint-Gobain S.A.). The reactor was proved stable after long-term use (18 months), although some of the ABS was found to have degraded over time, as discussed in Text S3.

2.3. Evaluation of the continuous sunlight/PS/Fe^{2+} system

The performance of the continuous system was evaluated in terms of the effects of the initial dose of the radical precursor (SPS) and the catalyst concentration (Fe^{2+}). The catalyst was chosen after preliminary tests (Text S2). The effects were investigated systematically by performing a multivariate response surface design based on the Doehlert matrix [8]. The design comprised a total of nine experiments, as presented in Table 2, including three replicates at the central point of the design in order to evaluate random errors and have a measurement of experimental uncertainty. The initial PS dose (X_1) was varied in five levels and the catalyst dose (X_2) was varied in three levels. The two reported response variables were the conversion achieved at a space time of 3.3 min (Y_1,%), and the pseudo-first order reaction rate for acetaminophen conversion (Y_2, min^{-1}).

In a typical experiment of the design, ~60.0 mL of a stock solution of SPS was collected in a PP syringe (Descarpack Ltd.), which was placed in the holder of the syringe pump. Next, a suitable amount of $FeSO_4$ $7H_2O$ was weighed and dissolved in the ACT stock solution, which was then transferred to a flask equipped with a sampling tube connected to the metering pump. Both the syringe and the outlet of the metering pump were connected to different ports of the static mixer attached to the metering pump, as shown in Fig. 1. The mixed stream (C_{ACT} = 5 mg L^{-1}, C_{SPS} and C_{Fe} as indicated in Table 2) was fed to the reactor, where the photoinduced transformations take place. The flow rates of both pumps were adjusted to control the overall volumetric flow rate passing through the reactor, which was set to vary at five levels: 300, 450, 600, 900 and 1200 μL min^{-1}. Considering the free volume of the reactor (3.0 mL), these flow rates correspond to space times of 10, 6.7, 5, 3.3 and 2.3 min, respectively. At each flow rate condition, 0.7-mL samples were collected at the reactor outlet and diluted with 0.3 mL of methanol to promote quenching of radical species. The samples were then stored in a dark and refrigerated environment (~5 °C) until the end of the experiment, when all samples were analyzed to quantify the remaining dose of acetaminophen. To ensure the steady-state of the outlet composition, the reactor was stabilized at each flow rate condition by allowing two reactor volumes (equivalent to two space-time intervals) to flow through the system before collecting the samples. Three samples were collected consecutively at each flow rate to verify steady-state operation. The temperature of the reactor was allowed to vary freely under the light source and would stabilize after ca. 10 min at approximately 39 ± 4 °C, while the room temperature was set at 23 °C. The initial temperatures of the working solutions were set at 10−12 °C, and were not controlled over the course of the experiment. As a consequence, the temperature of the solution at the outlet of the reactor would vary between 20−27 °C over the course of one experiment, depending on the flow rates used.

A validation experiment adopting the same conditions of the central point of the experimental design was carried out to confirm whether the simulated irradiance would represent natural irradiation conditions. In this experiment, the lamp shown in Fig. 1 was removed and the entire apparatus was placed on an open platform exposed to natural irradiation. Pumps and reservoirs (i.e. acetaminophen + $FeSO_4$ solution bottle and SPS-containing syringe) were placed inside an opaque container to prevent the occurrence of undesirable photochemical reactions. The experiment was carried out on August 20, 2021, a clear-sky winter day, at the laboratory for Advanced Oxidation Processes, in São Paulo, Brazil (23°33′48.6″S, 46°43′36.6″W), from 11:30 am to 1:30 pm (BRT). A spectroradiometer collected irradiance data minute-wise throughout the experiment. The average sunlight intensity within the UV-A bandwidth was measured as $I_{UV\text{-}A}$ = 5.17 mW cm^{-2}.

Batch experiments repeating the same conditions of the central point of the experimental design were carried out to compare the performance of the two operation modes (continuous vs. batch). In this experiment, the reactants were added to a 50 mL beaker under continuous magnetic stirring and exposed to lamp irradiation. The lamp was placed 15 cm above the liquid interface to ensure the same level of irradiance experienced in the continuous system. The reaction was carried out in triplicate for 30 min and 0.7-mL aliquots were collected at 2, 3, 5, 7, 10, 15, 20 and 30 min. The aliquots were diluted in 0.3 mL of methanol, as described above, and analyzed by HPLC.

Lastly, the dominant oxidative species were investigated in batch experiments using isopropanol and tert-butyl alcohol (TBA), as $HO^{\bullet}$ and $SO_4^{\bullet-}$ scavengers, and hydroquinone as a global radical scavenger. The assays were carried out in batch mode, with a total irradiation time of 15 min. In these experiments, test tubes were filled with 5 mL of a 5 mg L^{-1} ACT solution, with SPS at 1.65 mmol L^{-1}, and $FeSO_4$ at 0.138 mmol L^{-1}, reproducing the concentrations from the central point of the experimental design. Each of the radical scavengers was added in excess with respect to ACT, at an initial concentration of 200 mmol L^{-1} [11]. TBA is a preferential $HO^{\bullet}$ radical scavenger ($k_{HO\bullet}$ = 3.8–7.6 × 10^8 L mol^{-1} s^{-1}), and reacts slowly with $SO_4^{\bullet-}$ radicals ($k_{SO4\bullet-}$ = 4.0–9.1 × 10^5 L mol^{-1} s^{-1}) [12]; while isopropanol is a good scavenger of both radicals ($k_{HO\bullet}$ = 1.9 × 10^9 L mol^{-1} s^{-1} and $k_{SO4\bullet-}$ = 4.0 × 10^7 L mol^{-1} s^{-1}) [13,14].

2.4. Analytical procedures

The concentration of acetaminophen was quantified by UV absorbance (at 243 nm) after separation in a high precision liquid chromatography system (UFLC-20AD, Shimadzu Co.). Chromatographic separation was carried out in a reverse-phase column (Luna C18, 5 μm, 250 × 4.6 mm, Phenomenex Inc.) by isocratic elution of a 25:75 mixture of methanol and deionized water at a flow rate of 1.0 mL min^{-1} at 35 °C.

2.5. Mathematical modeling

To discuss the performance of the reaction system in both operating modes, a dynamic kinetic model was implemented in a mathematical software (Matlab 2022b, Mathworks Inc.). The model was based on the transient state molar balance of all species that participated in the generation and consumption of photogenerated radicals, listed in Table 1. Because of the continuous emission of photons along the length of the reactor, the photoreactor is essentially transient, and the equation for a transient plug flow photoreactor is described by Eq. III:

$$\frac{dC_i}{dt} = -\left(\frac{dC_i}{d\tau}\right) + \sum_j r_{ij} \quad \text{(III)}$$

where C_i is the concentration of species i, τ is the space time, and r_{ij} is the rate of consumption/generation of species i in reaction j. The reaction rates r_j are expressed assuming that all reactions described in Table 1 are elementary. To simplify the numerical evaluation, the continuous photoreactor was approximated as five (n = 5) equally irradiated continuous stirred tank reactors (CSTR) of the same volume arranged in series operating with a combined space time equivalent to each sampling point, as shown in Equation IV:

$$\frac{dC_{i,n}}{dt} = -\frac{(C_n - C_{n-1})}{\tau_n - \tau_{n-1}} + \sum_j r_{ij,n} \quad \text{(IV)}$$

The system of 15 stiff ordinary differential equations (Table S2) was solved using the ode15s solver [15], for each space time experimentally evaluated. The numeric concentration of the species as a function of each spatial time was calculated after these values reached the stationary concentration (after 600 s). The values of the second-order rate for

Table 1
Reactions involved in the Sunlight/PS/Fe^{2+} system for the oxidation of ACT.

No.	Reaction	Kinetic parameter	Reference
1a	$S_2O_8^{2-} \xrightarrow{h\nu} 2\ SO_4^{\bullet-}$	$\Phi_{SO_4^{\bullet-},350-370nm}$ (Fig. S1A) $\varepsilon_{S_2O_8^{2-},330-400\,nm}$(Fig. S2A)	[18] This study
1b	$S_2O_8^{2-} \xrightarrow{T} 2SO_4^{\bullet-}$	$E_A = 96$ kJ mol^{-1} $k_0 = 1.34 \times 10^{10}\ s^{-1}$	[19]
2	$SO_4^{\bullet-} + SO_4^{\bullet-} \rightarrow S_2O_8^{2-}$	$k_2 = 8.1 \times 10^8$ L mol^{-1} s^{-1}	[14]
3	$SO_4^{\bullet-} + S_2O_8^{2-} \rightarrow SO_4^{2-} + S_2O_8^{\bullet-}$	$k_3 = 1.2 \times 10^6$ L mol^{-1} s^{-1}	[14]
4	$SO_4^{\bullet-} + H_2O \rightarrow HSO_4^- + HO^{\bullet}$	$k_4 = 460\ s^{-1}$	[14]
5	$HSO_4^- + HO^{\bullet} \rightarrow SO_4^{\bullet-} + H_2O$	$k_5 = 6.9 \times 10^5$ L mol^{-1} s^{-1}	[14]
6	$SO_4^{\bullet-} + HO^- \rightarrow SO_4^{2-} + HO^{\bullet}$	$k_6 = 6.5 \times 10^7$ L mol^{-1} s^{-1}	[14]
7	$SO_4^{\bullet-} + HO^{\bullet} \rightarrow HSO_4^- + 0.5O_2$	$k_7 = 1.0 \times 10^{10}$ L mol^{-1} s^{-1}	[20]
8	$S_2O_8^{2-} + HO^{\bullet} \rightarrow HSO_4^- + SO_4^{\bullet-} + 0.5\ O_2$	$k_8 = 1.2 \times 10^7$ L mol^{-1} s^{-1}	[20]
9	$S_2O_8^{2-} + HO^{\bullet} \rightarrow S_2O_8^{\bullet-} + HO^-$	$k_9 = 1.4 \times 10^7$ L mol^{-1} s^{-1}	[13]
10	$HSO_4^- \rightarrow SO_4^{2-} + H^+$	$k_{10} = 1.0 \times 10^{10}\ s^{-1}$	[21]
11	$SO_4^{2-} + H^+ \rightarrow HSO_4^-$	$k_{11} = 4.5 \times 10^{11}$ L mol^{-1} s^{-1} $pk_a = 1.9$	[21]
12	$H_2O \rightarrow H^+ + OH^-$	$k_{12} = 1.14 \times 10^{-6}$ L mol^{-1} s^{-1}	[14]
13	$H^+ + OH^- \rightarrow H_2O$	$k_{13} = 1.0 \times 10^{10}\ s^{-1}$ $pk_a = 16$	[14]
14	$ACT + SO_4^{\bullet-} \rightarrow$ Products	$k_{14} = 1.8 \times 10^9$ L mol^{-1} s^{-1}	This study
15	$ACT + HO^{\bullet} \rightarrow$ Products	$k_{15} = 1.1 \times 10^9$ L mol^{-1} s^{-1}	This study
In the presence of Fe^{2+} and Fe^{3+}			
16	$Fe^{2+} + S_2O_8^{2-} \rightarrow Fe^{3+} + SO_4^{\bullet-} + SO_4^{2-}$	$k_{16} = 17$ L mol^{-1} s^{-1}	[3]
17	$Fe^{2+} + SO_4^{\bullet-} \rightarrow Fe^{3+} + SO_4^{2-}$	$k_{17} = 4.6 \times 10^9$ L mol^{-1} s^{-1}	[3]
18	$Fe^{2+} + HO^{\bullet} \rightarrow Fe^{3+} + OH^-$	$k_{18} = 3.2 \times 10^8$ L mol^{-1} s^{-1}	[3]
19	$Fe^{3+} + H_2O \rightarrow Fe(OH)^{2+} + H^+$	$k_{19} = 2.34 \times 10^7$ L mol^{-1} s^{-1}	[22]
20	$Fe(OH)^{2+} + H^+ \rightarrow Fe^{3+} + H_2O$	$k_{20} = 1.0 \times 10^{10}$ L mol^{-1} s^{-1}	[22]
21	$Fe^{3+} + SO_4^{2-} \rightarrow Fe(SO_4)^+$	$k_{21} = 2.1 \times 10^{12}$ L mol^{-1} s^{-1}	[22]
22	$Fe(SO_4)^+ \rightarrow Fe^{3+} + SO_4^{2-}$	$k_{22} = 1.0 \times 10^{10}\ s^{-1}$	[22]
23	$Fe^{3+} + 2SO_4^{2-} \rightarrow Fe(SO_4)_2^-$	$k_{23} = 1.9 \times 10^{13}$ L mol^{-1} s^{-1}*	[22]
24	$Fe(SO_4)_2^- \rightarrow Fe^{3+} + 2SO_4^{2-}$	$k_{24} = 1.0 \times 10^{10}\ s^{-1}$	[22]
25	$Fe^{2+} + SO_4^{2-} \rightarrow FeSO_4$	$k_{25} = 1.2 \times 10^{11}$ L mol^{-1} s^{-1}	[22]
26	$FeSO_4 \rightarrow Fe^{2+} + SO_4^{2-}$	$k_{26} = 1.0 \times 10^{10}\ s^{-1}$	[22]
27	$Fe^{3+} + 2H_2O \rightarrow Fe(OH)_2^+ + 2H^+$	$k_{27} = 4.7 \times 10^3\ s^{-1}$	[22]
28	$Fe(OH)_2^+ + 2H^+ \rightarrow Fe^{3+} + 2H_2O$	$k_{28} = 1.0 \times 10^{10}$ L mol^{-1} s^{-1}	[22]
29	$2Fe^{3+} + 2H_2O \rightarrow Fe_2(OH)_2^{4+} + 2H^+$	$k_{29} = 1.1 \times 10^7\ s^{-1}$	[22]
30	$Fe_2(OH)_2^{4+} + 2H^+ \rightarrow 2Fe^{3+} + 2H_2O$	$k_{30} = 1.0 \times 10^{10}$ L mol^{-1} s^{-1}	[22]
31a	$Fe(OH)^{2+} \xrightarrow{h\nu} Fe^{2+} + HO^{\bullet}$	$\Phi_{Fe(OH)^{2+},\ 350-370}$(Fig. S1B) $\varepsilon_{Fe(OH)^{2+},300-400}$ (Fig. S2B)	[23]
31b	$Fe(OH)_2^+ \xrightarrow{h\nu} Fe^{2+} + 2HO^{\bullet}$	$\Phi_{Fe(OH)_2^+,350-370}$(Fig. S1B) $\varepsilon_{Fe(OH)_2^+,300-400}$(Fig. S2B)	[23]
31c	$Fe_2(OH)_2^{4+} \xrightarrow{h\nu} 2Fe^{2+} + 2HO^{\bullet}$	$\Phi_{Fe_2(OH)_2^{4+},350-370}$(Fig. S1B) $\varepsilon_{Fe_2(OH)_2^{4+},300-400}$(Fig. S2B)	[23]
31d	$Fe(SO_4)^+ \xrightarrow{h\nu} Fe^{2+} + SO_4^{\bullet-}$	$\Phi_{Fe(SO_4)^+,\ 300-400}$ (Fig. S1A) $\varepsilon_{Fe(SO_4)^+,300-400nm}$ (Fig. S2B)	[23]
In the presence of TBA			
32	$TBA + SO_4^{\bullet-} \rightarrow$ Products	$k_{32} = 9.1 \times 10^5$ L mol^{-1} s^{-1}	[14]
33	$TBA + HO^{\bullet} \rightarrow$ Products	$k_{33} = 6.0 \times 10^8$ L mol^{-1} s^{-1}	[13]
In the presence of methanol			
34	$MeOH + SO_4^{\bullet-} \rightarrow$ Products	$k_{34} = 1.21 \times 10^7$ L mol^{-1} s^{-1}	[24]
35	$MeOH + HO^{\bullet} \rightarrow$ Products	$k_{35} = 9.70 \times 10^8$ L mol^{-1} s^{-1}	[24]
In the presence of hydroquinone			
36	$HQ + SO_4^{\bullet-} \rightarrow$Products	$k_{36} = 1.40 \times 10^9$ L mol^{-1} s^{-1}	[25]
37	$HQ + HO^{\bullet} \rightarrow$ Products	$k_{37} = 0.52$–2.10×10^{10} L mol^{-1} s^{-1}	[26]

* unit not clear in [22]

the reaction of ACT with $SO_4^{\bullet-}$ and $HO^{\bullet}$, radicals were estimated using a nonlinear least squares objective function executed using the Nelder-Mead simplex algorithm [16] to minimize the difference between the predicted and the measured concentration of ACT at each space time.

The rate of photolytic reactions can be described using a Beer-Lambertian model [17], as shown in Equations V and VI:

$$r_{UV,i} = \int \Phi_{i,\lambda} E_{P0,\lambda}\ \varepsilon_{i,\lambda}\ C_i f_\lambda\ d\lambda \tag{V}$$

$$f_\lambda = \left(\frac{1}{\sum \varepsilon_{i,\lambda} C_i}\right)\left(1 - 10^{-d_r \sum \varepsilon_{i,\lambda} C_i}\right) \tag{VI}$$

where $\Phi_{i,\lambda}$ is the spectral quantum yield of photoabsorbing species *i*; $E_{P0,\lambda}$ is the incoming photon flow; $\varepsilon_{i,\lambda}$ is the spectral extinction coefficient; f_λ is the fraction of transmitted light with wavelength λ; and d_r is the depth of the reactor (i.e. the optical length). This model neglects the light extinction effects of all species other than those involved in photochemical transformations. Table 1 summarizes the reactions considered in our experimental system.

.It is worth highlighting that other species present in wastewater may interact with the highly reactive radicals, inducing side reactions that might accelerate or slow down the degradation of acetaminophen in practical applications. Species such as dissolved organic matter, suspended solids, and inorganic ions (i.e. carbonates, phosphates, chlorides) are known to affect the kinetics of persulfate-based AOPs [27,28].

3. Results and discussion

3.1. Experimental design and photocatalytic performance

The investigation of the performance of the continuous Sunlight/PS/Fe^{2+} and its optimization were carried out using a response-surface experimental design to evaluate the optimum concentration of SPS and Fe to promote the highest conversion of ACT. The design consisted of nine experimental runs, as shown in Table 2, with two independent variables (X1 and X2) and two dependent variables (Y1 and Y2).

The ACT removal kinetics of the nine experiments of the Doehlert design are presented in Fig. 2A, for the five space-times explored. In all runs, the ACT removal was enhanced as the space time increased, as expected. An intermediate space time of 3.3 min was selected to evaluate the effects of the SPS and Fe^{2+} concentrations in the experimental design, resulting in the ACT conversions achieved shown in Fig. 2B. It can be seen that high degrees of conversion (94.1%, run 4) could be reached even in a short reaction time with suitable concentrations of SPS and catalyst. The lowest conversion was obtained in run 9, the experimental point with the least amount of catalyst and an intermediate concentration of SPS.

The response surface and the corresponding contour plot for the experimental design at a space time of 3.3 min are shown in Fig. 3. The ACT conversion increased with increasing $[SPS]_0$ and $[Fe^{2+}]_0$ until a certain point, and then started to decrease, suggesting that the optimal point for the Sunlight/PS/Fe^{2+} process should be within the experimental domain explored in the design. The enhancement in the pollutant removal as SPS and Fe^{2+} concentrations increase is expected,

Table 2
Doehlert experimental design.

Run number	Coded values X_1	X_2	Real values X_1: C_{SPS} (mM)	X_2: C_{Fe} (mM)	Responses Y_1: $X_{ACT,3.3}$	Y_2: k (min^{-1})
1	0	0	1.65	0.138	0.899 ± 0.015	0.5104 ± 0.021
2	0	0	1.65	0.138	0.871 ± 0.015	0.5536 ± 0.023
3	0	0	1.65	0.138	0.877 ± 0.015	0.5390 ± 0.022
4	1	0	3.00	0.138	0.941 ± 0.016	0.5762 ± 0.024
5	0.5	0.866	2.33	0.250	0.491 ± 0.008	0.1387 ± 0.006
6	−1	0	0.30	0.138	0.564 ± 0.009	0.2412 ± 0.010
7	−0.5	−0.866	0.98	0.025	0.470 ± 0.008	0.1976 ± 0.008
8	−0.5	0.866	0.98	0.250	0.662 ± 0.011	0.3309 ± 0.014
9	0.5	−0.866	2.33	0.025	0.427 ± 0.007	0.2503 ± 0.010

considering that more $HO^{\bullet}$ and $SO_4^{\bullet-}$ radicals are produced [1,11]. Nevertheless, an excess of Fe^{2+} ions in the system may cause excessive radical scavenging, since Fe^{2+} will react with $SO_4^{\bullet-}$ faster than their local generation (Reaction 17) [1]. This explains the decrease in ACT removal observed for $[Fe^{2+}]_0$ greater than 0.138 mmol L^{-1}. This result reinforces the importance of optimizing the dose of PS and Fe^{2+} in the system.

The inflection point observed in Fig. 3A indicated that the optimal values of the SPS and Fe^{2+} concentrations are close to the central point (runs 1–3), equivalent to $[SPS]_0 = 2.1$ mmol L^{-1} ($X_1 = 0.33$, coded) and $[Fe^{2+}]_0 = 0.14$ mmol L^{-1} ($X_2 = 0.05$, coded), shown as an open red circle in Fig. 3B. The Pareto chart (F test with $p < 0.005$), shown in Fig. 3C, illustrates that, for the studied range, both the SPS and Fe^{2+} concentrations had a significant influence on the conversion of ACT. The response surface model that predicts conversion as a function of $[SPS]_0$ and $[Fe^{2+}]_0$ is given by Eq. VI, with $R^2 = 0.819$. Further model data are given in Table S3.

$$X_{ACT,3.3}\ (\%) = 88.24 + 9.02X_1 + 7.39X_2 - 12.98X_1^2 - 44.98X_2^2 \quad \text{(VI)}$$

The apparent pseudo-first-order reaction rate (k) follows a similar trend, as shown in Fig. 4. The highest removal of ACT was equal to (94.1 ± 1.6)% (run 4), and the lowest was (42.7 ± 0.7)% (run 9), corresponding to pseudo-first-order kinetic constants of 0.576 ± 0.024 and 0.250 ± 0.010 min^{-1}, respectively. The optimal point, illustrated as an open circle marker in Fig. 4A, corresponds to a $C_{SPS} = 2.18$ mM and $C_{Fe} = 0.13$ mM, virtually the same as found for $X_{ACT,3.3}$, as expected.

The Pareto chart (F test with $p < 0.005$) in Fig. 4B shows that, within the experimental space explored, both PS and Fe^{2+} concentrations (linear and quadratic effects) have a significant influence on reaction rate. The response surface model is given by Eq. VII, with $R^2 = 0.8397$. The ANOVA data are reported in Table S4.

$$k\ (min^{-1}) = 0.534 + 0.089X_1 - 0.126X_1^2 - 0.365X_2^2 - 0.141X_1X_2 \quad \text{(VII)}$$

The progress of the reaction was attested by the appearance of new products on the LC chromatograms (e.g. Fig. S3), which could be attributed to oxidation intermediates such as quinones and hydroquinones, which are known to be formed by the decomposition of ACT under highly oxidative conditions [29].

3.2. Performance under natural sunlight (Proof-of-concept)

Fig. 5 shows the result of a validation experiment replicating the central point of the experimental design under natural sunlight. It can be seen that for all five space times evaluated, the performance under natural sunlight was not significantly different from that observed under simulated sunlight. Therefore, the ACT removal rates achieved under simulated sunlight ($k = 0.534 \pm 0.022$ min^{-1}) reproduce well the behavior under natural irradiation ($k = 0.482 \pm 0.020$ min^{-1}). By replacing simulated irradiation with natural sunlight, it is possible to drastically reduce costs and the environmental footprint. This result reinforces the fact that the continuous photo Fenton-like process using persulfate proposed here is an efficient system to remove organic pollutants of emerging concern. It is worth mentioning that the results were obtained on a clear-sky winter day ($I_{UV\text{-}A} = 5.17$ mW cm^{-2}). Naturally, it is expected that on cloudy days, the ACT removal rates will be significantly lower, as the incidence of sunlight would be mostly diffuse, leading to a decrease in UV rays and the intensity of visible light [30]. For example, Santana et al. [30] evaluated a photo-Fenton process under sunlight irradiation for the degradation of textile wastewater and observed a decrease of 18% in the degradation rate when natural sunlight was used, which was due to the occurrence of cloudy days during the experiments. However, when the assay was repeated but lasting

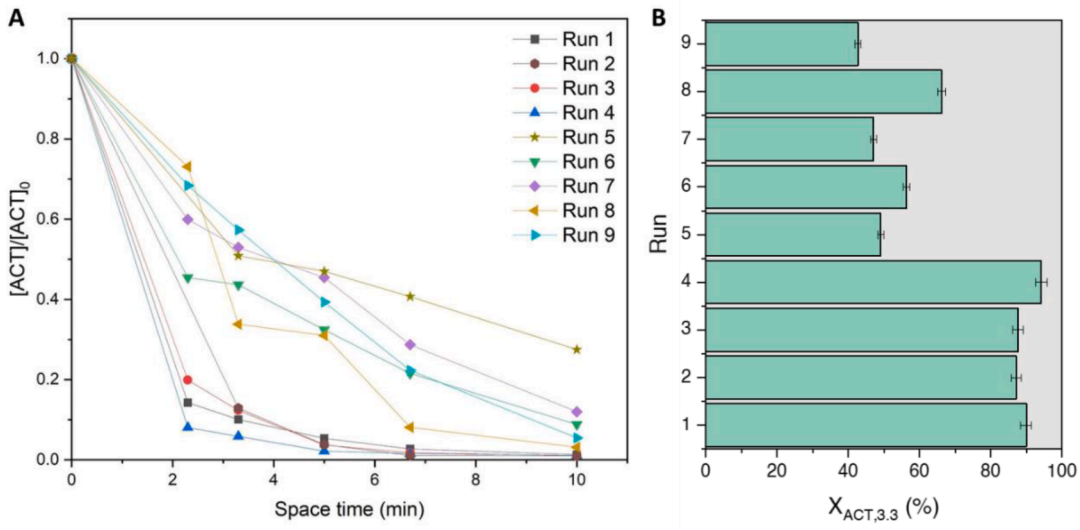

Fig. 2. ACT degradation kinetics. (A) Concentration profiles of each experiment for all explored space times; and (B) overall ACT conversion at the space time τ = 3.3 min. ($[ACT]_0 = 4.10 \pm 0.35$ mg L^{-1}).

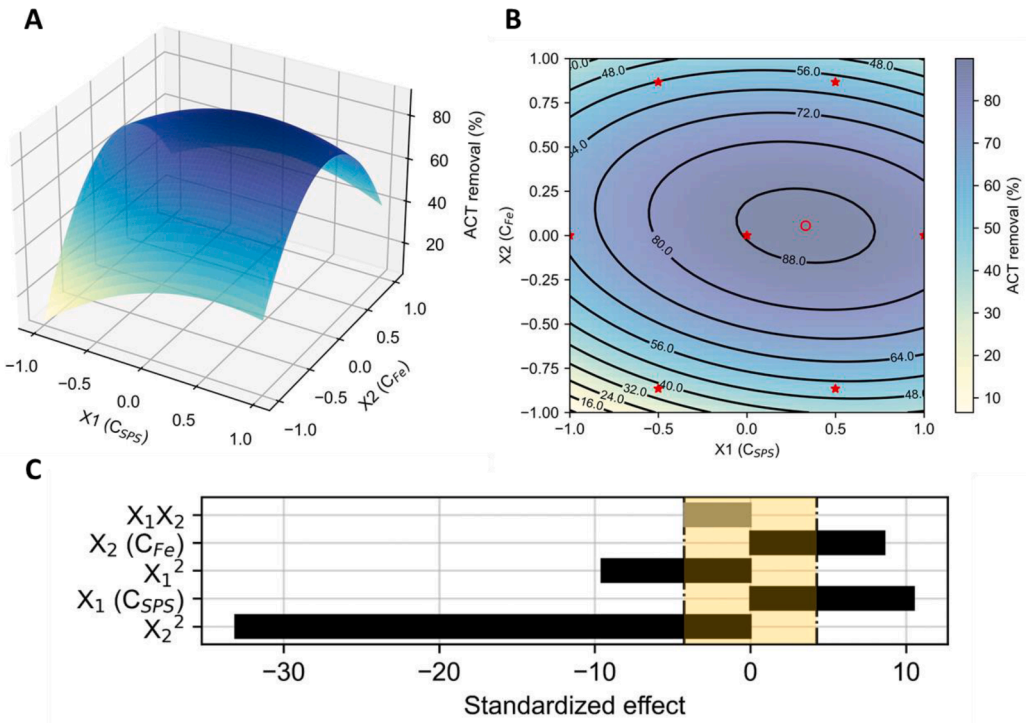

Fig. 3. Response surface analysis for the removal of ACT ($X_{ACT,3.3}$) in the Sunlight/PS/Fe^{2+}system. (A) Response surface and (B) contour plot with the experimental points (red stars). (C) Pareto chart of effects. ($[ACT]_0 = 4.10 \pm 0.35$ mg L^{-1}, and $\tau = 3.3$ min.).

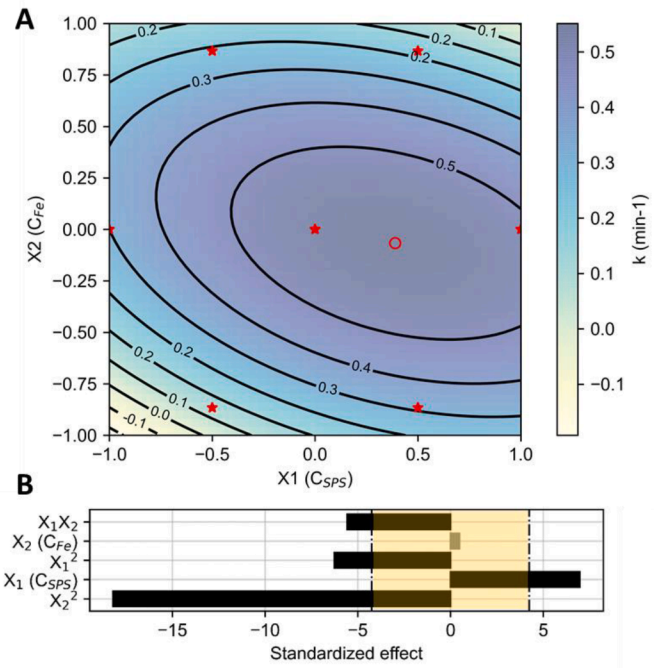

Fig. 4. Response surface analysis for the ACT removal kinetic constant (k, min^{-1}) in the Sunlight/PS/Fe^{2+}system. (A) Contour plot with the experimental points (red stars) and (D) Pareto chart of effects. ($[ACT]_0 = 4.10 \pm 0.35$ mg L^{-1}).

twice the original time, they could reach the same degradation rate found for the experiment performed using simulated sunlight.

3.3. Identification of active radicals and determination of their steady-state concentration

Lastly, experiments were carried out to understand the role of radicals formed in the Sunlight/PS/Fe^{2+} system. Fig. 6 shows that both isopropanol and TBA hindered ACT consumption, with the latter exerting a more pronounced effect. The experimental data followed a kinetic behavior consistent with a pseudo first-order model. *The k* values were equal to 0.379 ± 0.005 min^{-1} ($R^2 = 0.992$), 0.0960 ± 0.009 min^{-1} ($R^2 = 0.976$) and 0.0691 ± 0.002 min^{-1} ($R^2 = 0.974$) in the absence of scavengers and in the presence of TBA and isopropanol, respectively.

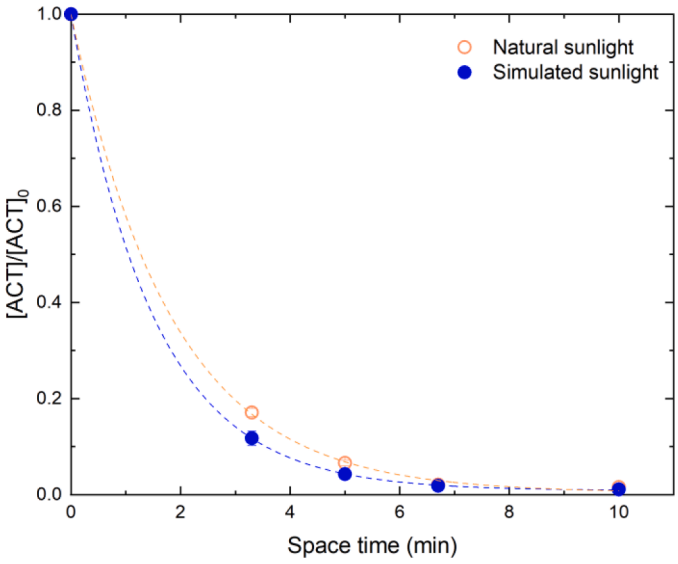

Fig. 5. ACT removal performance by Sunlight/PS/Fe^{2+}system, under simulated and natural sunlight. ($[ACT]_0$ = 5 ppm, $[SPS]_0$ = 1.65 mM, $[Fe^{2+}]_0$ = 0.138 mM).

Thus, ACT degradation was inhibited by approximately 74.6% for TBA and 81.8% for isopropanol, which means that both $HO^{\bullet}$ and $SO_4^{\bullet-}$ radicals play important roles in the reaction mechanism, although the latter seems to be more significant. In general, the reactions involved in sulfate-based AOPs for the degradation of various organic pollutants are driven mainly by $SO_4^{\bullet-}$ radicals, followed by hydroxyl radicals [31,32]. Reactions involving $SO_4^{\bullet-}$ radicals are favored because of its longer lifetime ($t_{1/2\ (SO4\bullet-)}$ = 30–40 μs and $t_{1/2\ (HO\bullet)}$ = 40 ns), resulting in a higher steady-state concentration and, thus, in higher contaminant removal [1]. It is also worth noting that ACT is still significantly degraded even in the presence of isopropanol and TBA. This suggests the presence of other reactive species, such as $^1O_2$ or $O_2^{\bullet-}$, likely produced by radical chemistry in aqueous systems, as competently discussed elsewhere [33,34].

The results obtained at the central points of the design for the continuous reactor and the batch experiment in the absence of scavengers were used to evaluate the second-order kinetic constants of ACT reactions with the radicals and to test the mathematical model using the mechanism given in Table 1 (Fig. S6). The simulations using these constants and considering the scavenging experiments indicate that the average radical concentration was of the order of 10^{-11} and 10^{-12} mol L^{-1} for the sulfate and hydroxyl radicals, respectively, in all experiments in the continuous reactor (Fig. 7A,B). In the batch experiments, the steady-state concentrations were reached after ~10 min of operation, around 10^{-12} mol L^{-1} for both radicals in the experiment carried out without scavengers, and substantially lower in experiments with the scavengers, as expected. The figure indicates that the concentration of sulfate radicals is approximately twice in the continuous system compared to the batch system under the same experimental conditions ($[ACT]_0 = 5$ ppm, $[PS]_0 = 1.65$ mM, $[Fe^{2+}]_0 = 0.138$ mM), while that of the hydroxyl radical was approximately one-sixth of the observed in the batch system. This suggests that the conversion of sulfate radicals into hydroxyl radicals was more pronounced in the batch operation, which can be attributed to their rapid initial production and consumption in this operation mode, as shown in Fig. 7C. The plug-flow-like fluid distribution in the continuous reactor [10] promotes the gradual formation of radicals along the reactor volume / residence time, as shown in Fig. 7E. This gradual formation resulted in an improved availability of sulfate radicals in the continuous operation mode, which could explain the faster kinetics observed in this system.

3.4. A final word on efficiency

The efficiency of a photochemical / photocatalytic process driven by sunlight can be evaluated in terms of the collector area per order (A_{CO}), as recommended by the IUPAC [35]. This figure of merit can be calculated for batch or continuous regimes as:

$$A_{CO} = \frac{A\overline{E}_S t}{E_S^0\, t^0\, V \log(1-X_t)^{-1}} = \frac{A\overline{E}_S}{E_S^0\, F \log(1-X_F)^{-1}} \qquad \text{(VIII)}$$

where A is the irradiated area (m^2); t is the treatment time (h), V is the treated volume (m^3), F is the flow rate ($m^3\ h^{-1}$), X_t and X_F are the conversions achieved at time t or the flow rate F, respectively; $\overline{E}_S$ and $\overline{E}_S^0$ (= 1000 W m^{-2}) are the average and standard integrated solar irradiances (W m^{-2}), respectively. This parameter is particularly useful for comparing different systems, regardless of size or geometry.

Applying Eq. VIII in our system, the A_{CO} was evaluated at 11.4 m^2 per (m^3 order). This indicates that it is possible to treat 1 m^3 of effluent to remove 90% of the initial ACT dose (~5 ppm) using a total irradiated area of 11.4 m^2 with a residence time of 3.3 min. This figure, with

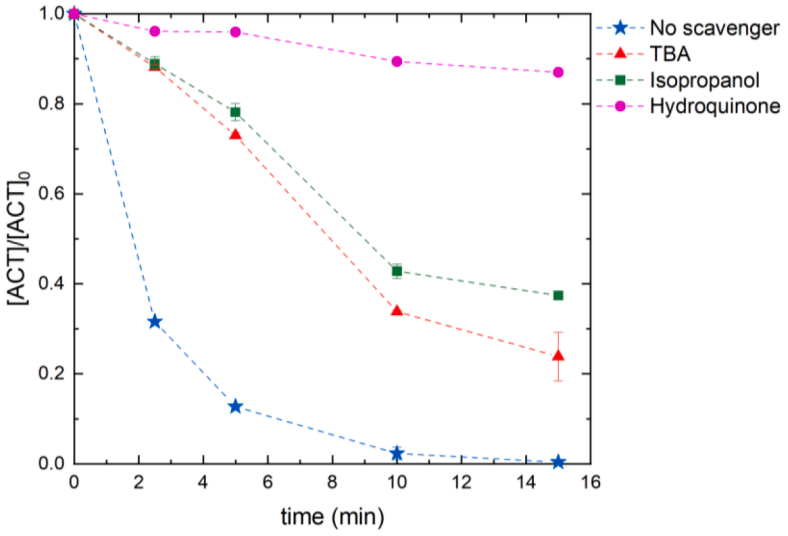

Fig. 6. Effect of radical scavengers on the removal of ACT by the Sunlight/PS/Fe^{2+}system, in batch mode. ($[ACT]_0 = 5$ ppm, $[PS]_0 = 1.65$ mM, $[Fe^{2+}]_0 = 0.138$ mM, $[Scavenger]_0$ = 200 mM).

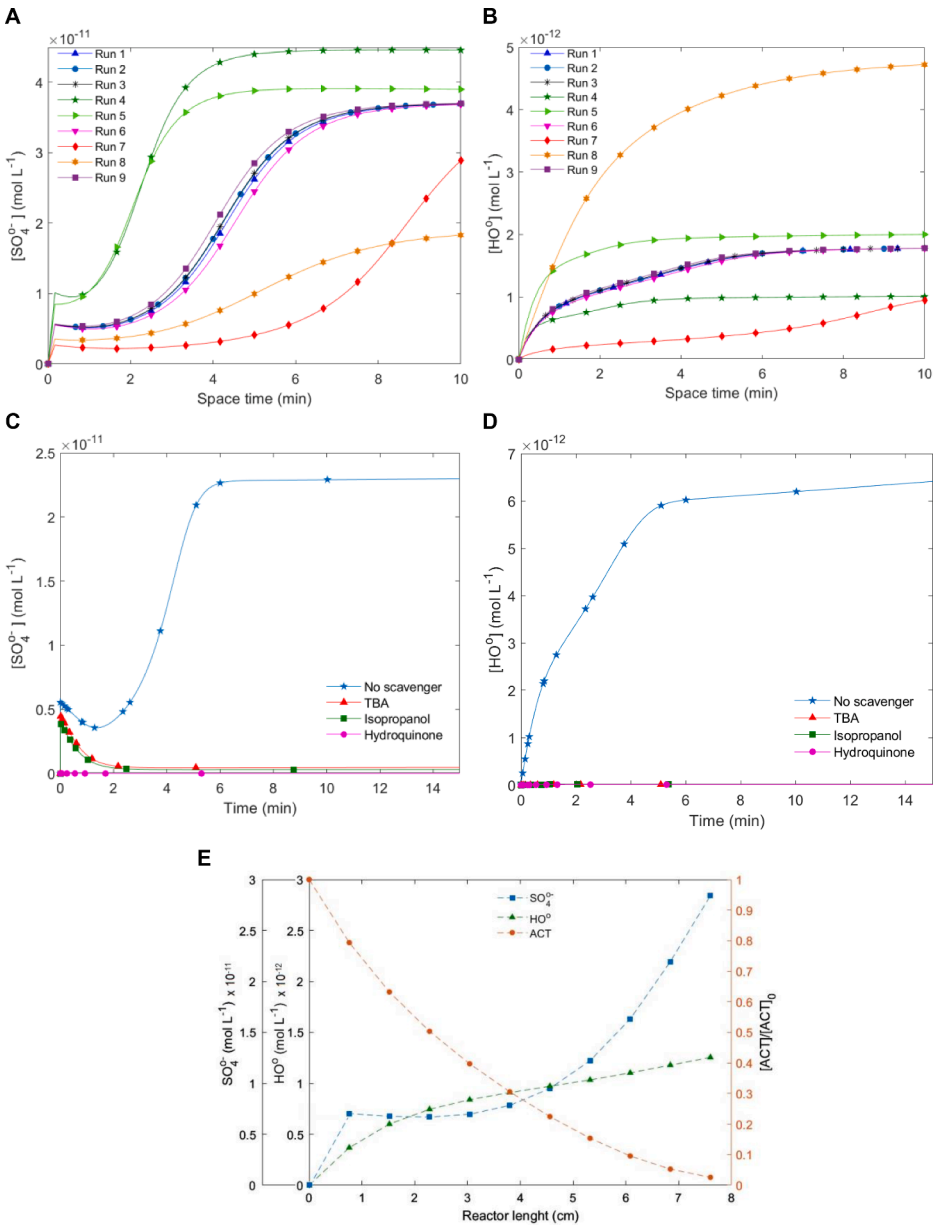

Fig. 7. Steady-state concentration of sulfate radicals (A, C) and hydroxyl radicals (B, D) radicals as a function of the irradiation (space) time in the continuous reactor for the 9 experiments of the Doehlert design (A, B) and in the batch experiments (C, D). (E) Concentration profile of the relevant radicals and ACT in the continuous reactor at $\tau = 3.3$ min. (Batch experiments, Runs 1–3 and E: $[ACT]_0 = 5$ ppm, $[PS]_0 = 1.65$ mM, $[Fe^{2+}]_0 = 0.138$ mM, $pH_0 = 5.6$).

related data, is listed in Table 3, along with the few works reported on solar-driven processes to treat ACT-contaminated water. Nasr et al. [36] developed modified TiO_2 nanoparticles for use in sunlight-driven photocatalysis, and using a batch system obtained A_{CO} ranging from 48 to 74 $m^2\ m^{-3}$ $order^{-1}$, for samples doped with 1% Pt and the undoped catalyst, respectively. On the other hand, Gimenez et al. [37] investigated a system similar to ours, consisting of a flat-plate solar reactor that runs the photo-Fenton system at circumneutral pH, but using H_2O_2 as auxiliary oxidant instead of persulfate. His-system had a performance of ~23.5 $m^2\ m^{-3}$ $order^{-1}$, but operated in a batch regime, which could explain the poorer efficiency compared to ours. Jimenez et al. [38] studied modified tubular reactors for solar degradation of ACT using TiO_2 and found that the incorporation of static mixers improved the performance of the system. The A_{CO} figure of their reaction systems varied from 20 to 40 $m^2\ m^{-3}$ $order^{-1}$, depending on the number of mixing sections used. Lastly, Almeida et al. [39] designed a hybrid electrochemical-solar reactor to treat a 150 ppm solution of ACT using a combination of electrochemical and photo-Fenton processes. The A_{CO} of their system is very similar to ours, at 11.3 m^2 per (m^3 order) when operating under the optimized conditions. These results show that our solution is well aligned with the best cases offered in the literature for sunlight-driven AOPs.

4. Conclusion

In the growing race toward sustainability, the chemical industry is looking for new processes that minimize energy consumption, waste generation, and footprint. Furthermore, when wastewater and water treatment is considered, new processes must be able to operate in a continuous regime to facilitate integration into the existing process pipeline. This paper reported the development of a process that approaches these four requirements, by (i) replacing energy-intensive and costly UV-C lamps with natural sunlight, (ii) minimizing waste generation by using optimal amounts of inorganic salts as catalysts that can be

Table 3
Figure of merit of ACT degradation in sunlight-driven AOPs. A_{CO} refers to the *collector area per order* (see text). The information in this table was calculated using data from the references.

System	ACT conversion	Irradiated area (m^2)	Average solar irradiance (kW m^{-2})	A_{CO} (m^2 m^{-3} $order^{-1}$)	Ref.
Sunlight/PS/Fe^{2+} Continuous flat-plate reactor	94% (3.3 min)	1.0×10^{-3}	750	11.4	This work
TiO_2 batch tank reactor	79% (120 min)	1.3×10^{-3}	850	63.0	[36]
1% Ag-TiO_2 batch tank reactor	89% (120 min)	1.3×10^{-3}	850	44.6	[36]
1% Au-TiO_2 batch tank reactor	85% (120 min)	1.3×10^{-3}	850	51.9	[36]
1% Pt-TiO_2 batch tank reactor	91% (120 min)	1.3×10^{-3}	850	40.9	[36]
Photo-Fenton batch flat-plate reactor	91% (90 min)	0.24	205	23.5	[37]
TiO_2 batch CPC tubular reactor	56% (no mixer)[1] 68% (100% with mixer) 80% (50% with mixer) (t = 180 min)	0.8	174	39.0 (no mixer) 28.1 (100% with mixer) 20.0 (50% with mixer)	[38]
SPEF[2] batch CPC tubular reactor + filter press electrochemical reactor	85% (30 min)	0.4	464	11.3	[39]

[1] percentage of tubes equipped with a static mixer.
[2] solar photoelectro-Fenton.

safely disposed of, and (iii) achieving high efficiency to reach minimal A_{CO}.

Using a 3D printed prototype made from recycled plastic waste, we reported a proof-of-concept development of an intensified flat-plate reactor-based system based on the sunlight activation of persulfate aided by ferrous salts capable of operating in a continuous regime. Based on a multivariate response surface design, we evaluated the performance of a continuous Sunlight/PS/Fe^{2+}system in terms of the effects of the initial dose of the radical precursor (SPS) and the concentration of the catalyst (Fe^{2+}). We showed that using suitable concentrations of SPS and catalyst, high conversion rates (>90%) can be achieved even in less than 5 min of exposure time. A validation experiment confirmed that the simulated sunlight we used in the experiments represents natural sunlight to a good extent.

Batch experiments replicating the central point of the experimental design and a dynamic kinetic model indicated that continuous operation allowed for higher conversions than the batch regime and a key aspect controlling the superior performance of the continuous system was the higher steady-state concentration of sulfate radicals.

Finally, we show that the efficiency of our continuous sunlight-driven system, evaluated in terms of the collector area per order (A_{CO}), is superior to most reported data on sunlight-driven AOPs for acetaminophen removal, virtually equal to that of an expensive photoelectrochemical process. This figure indicates that our system is technologically competitive and is a strong candidate for further upscaling efforts.

Ethics approval and consent to participate

Not applicable.

Consent for publication

Not applicable.

Availability of data and materials

The data sets used and/or analyzed during the current study are available from the corresponding author on reasonable request.

Funding

This work has received the support of the São Paulo Research Foundation (FAPESP grant 18/21271–6) for the acquisition of equipment and materials. The authors were supported by the National Council for Scientific and Technological Development (CNPq), Coordenação de Aperfeiçoamento de Pessoal de Nível Superior – Brasil (CAPES), and Sao Paulo Research Foundation (FAPESP grants 21/10919–8 and 19/05840–3) with research fellowships. This study was financed in part by the Coordenação de Aperfeiçoamento de Pessoal de Nível Superior – Brasil (CAPES) – Finance Code 001 through provision of institutional infrastructure.

CRediT authorship contribution statement

Bruno Ramos: Conceptualization, Methodology, Data curation, Formal analysis, Writing – original draft, Supervision. **Lívia Babetto Ferreira:** Methodology, Data curation, Formal analysis. **Priscila Hasse Palharim:** Conceptualization, Methodology, Formal analysis, Writing – original draft. **Patrícia Metolina:** Writing – original draft. **Carolina de Araújo Gusmão:** Formal analysis, Writing – original draft. **Antonio Carlos Silva Costa Teixeira:** Supervision, Project administration, Funding acquisition, Writing – original draft.

Declaration of Competing Interest

The authors declare that they have no known competing financial interests or personal relationships that could have appeared to influence the work reported in this paper.

Data availability

Data will be made available on request.

Acknowledgments

The authors would like to acknowledge the funding of the aforementioned institutions. We also thank Mr. William Lima of PrintGreen 3D for kindly providing the recycled ABS filament for 3D printing our prototypes.

Supplementary materials

Supplementary material associated with this article can be found, in the online version, at doi:10.1016/j.ceja.2023.100473.

References

[1] A.V. Karim, Y. Jiao, M. Zhou, P.V. Nidheesh, Iron-based persulfate activation process for environmental decontamination in water and soil, Chemosphere 265 (2021), https://doi.org/10.1016/j.chemosphere.2020.129057, 129057–12077.

[2] Y. Gao, P. Champagne, D. Blair, O. He, T. Song, Activated persulfate by iron-based materials used for refractory organics degradation: a review, Water Sci. Technol. 81 (2020) 853–875, https://doi.org/10.2166/wst.2020.190.

[3] H. Kusic, I. Peternel, S. Ukic, N. Koprivanac, T. Bolanca, S. Papic, A.L. Bozic, Modeling of iron activated persulfate oxidation treating reactive azo dye in water matrix, Chem. Eng. J. 172 (2011) 109–121, https://doi.org/10.1016/j.cej.2011.05.076.

[4] J.A. Khan, X. He, H.M. Khan, N.S. Shah, D.D. Dionysiou, Oxidative degradation of atrazine in aqueous solution by UV/H_2O_2/Fe^{2+}, UV/$S_2O_8^{2-}$/Fe^{2+} and UV/HSO_5^-/Fe^{2+} processes: a comparative study, Chem. Eng. J. J. 218 (2013) 376–383, https://doi.org/10.1016/j.cej.2012.12.055.

[5] M.M. Ahmed, S. Chiron, Solar photo-Fenton like using persulphate for carbamazepine removal from domestic wastewater, Water Res. 48 (2013) 229–236, https://doi.org/10.1016/j.watres.2013.09.033.

[6] E.R. Bandala, Z. Domínguez, F. Rivas, S. Gelover, Degradation of atrazine using solar driven fenton-like advanced oxidation processes, J. Environ. Sci. Heal. Part B. 42 (2007) 21–26, https://doi.org/10.1080/03601230601017965.

[7] M. Nie, C. Yan, X. Xiong, X. Wen, X. Yang, Degradation of chloramphenicol using a combination system of simulated solar light, Fe^{2+} and persulfate, Chem. Eng. J. 348 (2018) 455–463, https://doi.org/10.1016/j.cej.2018.04.124.

[8] D.H. Doehlert, Uniform shell designs, Appl. Stat. 19 (1970) 231–239, https://doi.org/10.2307/2346327.

[9] C.A. Gueymard, The sun's total and spectral irradiance for solar energy applications and solar radiation models, Sol. Energy. 76 (2004) 423–453, https://doi.org/10.1016/j.solener.2003.08.039.

[10] B. Ramos, J.G.M. Carneiro, L.I. Nagamati, A.C.S.C. Teixeira, Development of intensified flat-plate packed-bed solar reactors for heterogeneous photocatalysis, Environ. Sci. Pollut. Res. 28 (2021) 24023–24033, https://doi.org/10.1007/s11356-020-11806-9.

[11] P.H. Palharim, M.C.D. Caira, C.A. Gusmão, B. Ramos, G.T. dos Santos, O. Rodrigues, A.C.S.C. Teixeira, Effect of temperature and time on the hydrothermal synthesis of WO_3-AgCl photocatalysts regarding photocatalytic activity, Chem. Eng. Res. Des. 188 (2022) 935–953, https://doi.org/10.1016/j.cherd.2022.10.045.

[12] D. Han, J. Wan, Y. Ma, Y. Wang, Y. Li, D. Li, Z. Guan, New insights into the role of organic chelating agents in Fe (II) activated persulfate processes, Chem. Eng. J. 269 (2015) 425–433, https://doi.org/10.1016/j.cej.2015.01.106.

[13] G.V. Buxton, C.L. Greenstock, W.P. Helman, A.B. Ross, Critical Review of rate constants for reactions of hydrated electrons, hydrogen atoms and hydroxyl radicals (·OH/·O− in Aqueous Solution, J. Phys. Chem. Ref. Data. 17 (1988) 513–886, https://doi.org/10.1063/1.555805.

[14] P. Neta, R.E. Huie, A.B. Ross, Rate constants for reactions of inorganic radicals in aqueous solution, J. Phys. Chem. Ref. Data. 17 (1988) 1027–1284, https://doi.org/10.1063/1.555808.

[15] O.A. Akinfenwa, S.N. Jator, N.M. Yao, Continuous block backward differentiation formula for solving stiff ordinary differential equations, Comput. Math. with Appl. 65 (2013) 996–1005, https://doi.org/10.1016/j.camwa.2012.03.111.

[16] I. Fajfar, J. Puhan, B. Árpád, The Nelder–Mead simplex algorithm with perturbed centroid for high-dimensional function optimization, Optim. Lett. 13 (2018) 1011–1025, https://doi.org/10.1007/s11590-018-1306-2.

[17] S. Parsons, Advanced oxidation processes for water and wastewater treatment, 2005. https://doi.org/10.2166/9781780403076.

[18] H. Herrmann, On the photolysis of simple anions and neutral molecules as sources of O^-/OH, SO_x^- and Cl in aqueous solution, Phys. Chem. Chem. Phys. 9 (2007) 3935–3964, https://doi.org/10.1039/b618565g.

[19] V.C. Mora, J.A. Rosso, D.O. Mártire, M.C. Gonzalez, Phenol depletion by thermally activated peroxydisulfate at 70°C, Chemosphere 84 (2011) 1270–1275, https://doi.org/10.1016/j.chemosphere.2011.04.062.

[20] J. Criquet, N.K.V. Leitner, Degradation of acetic acid with sulfate radical generated by persulfate ions photolysis, Chemosphere 77 (2009) 194–200, https://doi.org/10.1016/j.chemosphere.2009.07.040.

[21] A. Rubio-Clemente, E. Chica, G.A. Peñuela, Kinetic model describing the UV/H_2O_2 photodegradation of phenol from water, Chem. Ind. Chem. Eng. Q. 23 (2017) 547–562, https://doi.org/10.2298/CICEQ161119008R.

[22] A. Machulek Jr., F.H. Quina, F. Gozzi, V.O. Silva, L.C. Friedrich, J.E.F. Moraes, Fundamental mechanistic studies of the Photo-Fenton reaction for the degradation of organic pollutants, in: org. Pollut, Ten Years After Stock. Conv. (2012) 271–294, https://doi.org/10.5772/30995.

[23] H. Benkelberg, P. Warneck, Photodecomposition of iron (III) hydroxo and sulfato complexes in aqueous solution: wavelength dependence of OH and SO_4^- quantum yields, J. Phys. Chem. 99 (1995) 5214–5221, https://doi.org/10.1021/j100014a049.

[24] S. Wang, J. Wu, X. Lu, W. Xu, Q. Gong, J. Ding, B. Dan, P. Xie, Removal of acetaminophen in the Fe^{2+}/persulfate system: kinetic model and degradation pathways, Chem. Eng. J. 358 (2019) 1091–1100, https://doi.org/10.1016/j.cej.2018.09.145.

[25] Python Simulator of Rate Constant. https://doi.org/http://www.pysirc.com.br/, 2022 (acessed 10 October 2022).

[26] A.A. Al-Suhybani, G. Hughes, Pulse radiolysis of deaerated hydroquinone solutions, J. Chem. Soc. Pakistan. 8 (1986) 107–115.

[27] R.F. Nunes, P. Metolina, A.C.S.C. Teixeira, Dodecylpyridinium chloride removal by persulfate activation using UVA radiation or temperature: experimental design and kinetic modeling, Environ. Sci. Pollut. Res. 28 (2021) 68229–68243, https://doi.org/10.1007/s11356-021-15174-w.

[28] Y. Zhao, Y. Zhao, Q. Li, R. Zhou, X. Chen, Effect of common inorganic ions on aniline degradation in groundwater by activated persulfate with ferrous iron, Water Sci. Technol. Water Supply 16 (2016) 667–674, https://doi.org/10.2166/ws.2015.174.

[29] M. Pacheco-Álvarez, R. Picos Benítez, O.M. Rodríguez-Narváez, E. Brillas, J. M. Peralta-Hernández, A critical review on paracetamol removal from different aqueous matrices by Fenton and Fenton-based processes, and their combined methods, Chemosphere 303 (2022) 34883–134909, https://doi.org/10.1016/j.chemosphere.2022.134883.

[30] R.M.R. Santana, D.C. Napoleão, S.G. dos Santos Júnior, R.K.M. Gomes, N.F.S. de Moraes, L.E.M.C. Zaidan, D.R.M. Elihimas, G.E. do Nascimento, M.M.M.B. Duarte, Photo-Fenton process under sunlight irradiation for textile wastewater degradation: monitoring of residual hydrogen peroxide by spectrophotometric method and modeling artificial neural network models to predict treatment, Chem. Pap. 75 (2021) 2305–2316, https://doi.org/10.1007/s11696-020-01449-y.

[31] P.H. Palharim, C.A.L. Graça, A.C.S.C. Teixeira, Comparison between UVA- and zero-valent iron-activated persulfate processes for degrading propylparaben, Environ. Sci. Pollut. Res. 27 (2020) 22214–22224, https://doi.org/10.1007/s11356-020-08141-4.

[32] Y. Chen, P. Deng, P. Xie, R. Shang, Z. Wang, S. Wang, Heat-activated persulfate oxidation of methyl- and ethyl-parabens: effect, kinetics, and mechanism, Chemosphere 168 (2017) 1628–1636, https://doi.org/10.1016/j.chemosphere.2016.11.143.

[33] D. Huang, W. Xu, L. Lei, S. Chen, C. Lai, W. Zhou, Y. Chen, R. Li, Promoted generation strategies and corresponding roles of singlet oxygen in activation of persulfate by nanoscale zero-valent iron systems, Chem. Eng. J. 449 (2022) 137493–137505, https://doi.org/10.1016/j.cej.2022.137493.

[34] J. Li, L. Yang, B. Lai, C. Liu, Y. He, G. Yao, N. Li, Recent progress on heterogeneous Fe-based materials induced persulfate activation for organics removal, Chem. Eng. J. 414 (2021) 128674–128705, https://doi.org/10.1016/j.cej.2021.128674.

[35] J.R. Bolton, K.G. Bircher, W. Tumas, C.A. Tolman, Figures-of-merit for the technical development and application of advanced oxidation technologies for both electric- and solar-driven systems, Pure Appl. Chem. 73 (2001) 627–637, https://doi.org/10.1351/pac200173040627.

[36] O. Nasr, O. Mohamed, A.-.S. Al-Shirbini, A.-.M. Abdel-Wahab, Photocatalytic degradation of acetaminophen over Ag, Au and Pt loaded TiO2 using solar light, J. Photochem. Photobiol. A Chem. 374 (2019) 185–193, https://doi.org/10.1016/j.jphotochem.2019.01.032.

[37] B.N. Giménez, L.O. Conte, O.M. Alfano, A.V. Schenone, Paracetamol removal by photo-Fenton processes at near-neutral pH using a solar simulator: optimization by ᴅ-optimal experimental design and toxicity evaluation, J. Photochem. Photobiol. A Chem. 397 (2020) 112584–112592, https://doi.org/10.1016/j.jphotochem.2020.112584.

[38] M.D. Jiménez, R.S. Galindo, C.A. Guevara, A.A. García, D.A.M. Montijo, Effect of the implementation of static mixers in a CPC solar reactor for the photocatalytic degradation of paracetamol, Top. Catal. 65 (2022) 980–988, https://doi.org/10.1007/s11244-022-01686-3.

[39] L.C. Almeida, S. Garcia-Segura, N. Bocchi, E. Brillas, Solar photoelectro-Fenton degradation of paracetamol using a flow plant with a Pt/air-diffusion cell coupled with a compound parabolic collector: process optimization by response surface methodology, Appl. Catal. B Environ. 103 (2011) 21–30, https://doi.org/10.1016/j.apcatb.2011.01.003.